Dirac nodal line induced anomalous low-energy acoustic plasmons on beryllium (0001) surface

Ronghan Li,[*] Jiangxu Li,[*] Peitao Liu, Yan Sun, and Xing-Qiu Chen[†]
Shenyang National Laboratory for Materials Science, Institute of Metal Research, Chinese Academy of Science, 110016 Shenyang, Liaoning, People's Republic of China
and School of Materials Science and Engineering, University of Science and Technology of China, Shenyang 110016, People's Republic of China

(Received 1 February 2023; accepted 25 April 2023; published 5 May 2023)

Beryllium is a simple hexagonal metal but exhibits anomalous low-energy acoustic plasmons on its (0001) surface, which are radically distinct from the conventional metal surface plasmons. Although the plasmons on Be(0001) have been extensively studied, the underlying mechanism remains elusive. Here, through first-principles calculations combined with model analysis, we unambiguously demonstrate that it is the topological Dirac nodal line induced surface states that result in the anomalous low-energy acoustic plasmons on Be(0001), rather than the commonly believed Shockley surface states. Our study not only clarifies the origin of the puzzling anomalous plasmons on Be(0001), but also provides a sound theoretical interpretation for the appearance of low-energy acoustic surface plasmons on the noble metal (111) surfaces. This work suggests that the topological nodal line semimetals offer a potential platform for obtaining low-energy acoustic plasmons.

DOI: 10.1103/PhysRevB.107.195408

A plasmon is a collective oscillation of charge density due to the long-range Coulomb interaction and an intrinsic property of three-dimensional (3D) metals [1] and metal surfaces [2]. The plasmons on the normal metal surfaces usually show very high frequencies (over 20 eV) and have thus been widely applied to surface dynamics [3,4], microscopy [5,6], and subwavelength optics [7–9]. In the two-dimensional (2D) nearly-free-electron-gas systems, the plasmons exhibit low frequencies (<5 eV) [10–13] and the frequencies are proportional to the square root of the incident momentum [10]. These plasmons are referred to as 2D plasmons. The typical examples of the 2D plasmons are those appearing in silicon inversion layers [11] and artificial layered materials [12,13].

In contrast to the 2D plasmons, the low-energy acoustic surface plasmons were observed on the (0001) surface of beryllium and the (111) surfaces of noble metals [14]. Because of the low-energy excitations and linear-dispersion nature, these acoustic surface plasmons exhibit very peculiar physical properties. They can participate in many low-temperature dynamical processes involving electrons and phonons, such as the electron-hole and electron-phonon dynamics near the Fermi level to mediate the formation of Cooper pairs in superconductors [13]. Although both the 2D plasmons and acoustic surface plasmons show low excitation frequencies, the latter are more effective in those low-temperature dynamical processes due to their soundlike long-wavelength dispersion relationships.

Due to the Coulomb screening effect of bulk electrons, on the surfaces of normal metals the low-energy excitations are usually suppressed [15] and only the conventional surface plasmons with very high frequencies form [2]. Therefore, the appearance of the low-energy acoustic plasmons on the Be(0001) surface [14,16–18] and the (111) surface of noble metals [14] is somewhat unexpected. These unusual phenomena have been intensively investigated in the past decades. To obtain a surface plasmon solution for the low-energy linear mode, Chaplik [19] first proposed a model by incorporating the 3D long-range dynamical screened Coulomb interactions into the 2D electron gas. Afterward, the 2D electron gas–like surface states, i.e., the Shockley surface states, were observed on the Be(0001) surface [20–25]. It was then recognized that the Be(0001) surface is a perfect system that can be well explained by Chaplik's model [19]. Later on, the anomalous low-energy acoustic plasmons on the Be(0001) surface were theoretically predicted [16,17] and experimentally observed by angle-resolved electron energy loss spectroscopy [14].

Only very recently has it become clear that the Shockley surface states were in fact topological nontrivial half-filled drumhead-like surface states (called DNSSs) on the (0001) surface induced by the topological Dirac nodal line (DNL) [26,27]. Now the common belief is that the formation of the low-energy acoustic plasmons was attributed to the anomalous localization of surface electrons [20–25], and the anomalous localization of such surface states is caused by the topological feature of the bulk bands. However, it remains elusive how the low-energy acoustic plasmons are mechanically connected with the surface state localization. Furthermore, although the surface plasmons have been extensively studied in topological insulators and Weyl semimetals [28–50], the studies of the surface plasmons in topological nodal-line materials are quite rare [51].

Here, through first-principles calculations and model analysis, we calculate the electronic structure and surface response function on the Be(0001) surface. From the derived surface

[*]These authors contributed equally to this work.
[†]xingqiu.chen@imr.ac.cn

band structure, we identify the topological Dirac nodal line induced surface states (DNSSs) close to the Fermi level and find that the DNSSs are highly localized on the Be(0001) surface. Our calculated surface plasmon dispersion relationships agree well with the experimental results [14] and previous *ab initio* calculations [17]. Moreover, our calculations reveal the anisotropic nature of the surface plasmon dispersion relationships on Be(0001), which, however, cannot be described by the one-dimensional (1D) potential model using a full nonlocal 3D dynamical screening [14,16–18]. By disentangling the contributions of the DNSSs from the states of the whole slab to the electron excitation rate of the surface plasmons, we show that the electron excitations from the DNSSs play a dominant role in the emergence of the anomalous low-energy acoustic plasmons on Be(0001).

The first-principles density functional theory (DFT) [52,53] calculations were carried out using the Vienna *ab initio* simulation package [54]. The Perdew-Burke-Ernzerhof exchange-correlation potential [55] was used. The plane-wave cutoff energy for the orbitals was set as 400 eV. The structure was optimized until the forces were less than 0.001 eV/Å, and the obtained lattice constants ($a = 2.263$ Å and $c = 3.573$ Å) are in good agreement with previous results [56,57]. The surface response function of the Be(0001) surface was computed using a 12-layer slab model with a vacuum width of 17.85 Å. A very dense k-point grid of $96\times96\times1$ was employed for the Brillouin zone (BZ) integration.

In order to obtain the surface plasmon spectral functions, we calculated the surface response function $g(\omega, \boldsymbol{q})$ at frequency ω and momentum $\boldsymbol{q}$ by [58]

$$g(\omega, \boldsymbol{q}) = \int dz\, e^{\boldsymbol{q}\cdot z} \int dz'\, \chi_{\mathbf{G},\mathbf{G}'}(z, z', \boldsymbol{q}, \omega) V_{\text{ext}}(z', \boldsymbol{q}, \omega). \quad (1)$$

Here, the atomic units ($e^2 = \hbar = m_e = 1$) were used. The integration over the coordinate $z$was performed from $-0.5c$ to $0.5c$ with c being the lattice constant of bulk Be in the z direction (3.573 Å). $\mathbf{G}$ denotes the reciprocal lattice vector. V_{ext} is the external potential, which has the form of $V_{\text{ext}}(z', \boldsymbol{q}, \omega) = -\frac{2\pi}{q} e^{\boldsymbol{q}\cdot z'}$, and $\chi_{\mathbf{G},\mathbf{G}'}(z, z', \boldsymbol{q}, \omega)$ is the nonlocal frequency-dependent interacting density response function, which can be obtained by solving the following Dyson-like equation within the framework of random-phase approximation and time-dependent density-functional theory,

$$\chi_{\mathbf{G},\mathbf{G}'}(\boldsymbol{q}, \omega) = \chi^0_{\mathbf{G},\mathbf{G}'}(\boldsymbol{q}, \omega) + \sum_{\mathbf{G}''} \chi^0_{\mathbf{G},\mathbf{G}''}(\boldsymbol{q}, \omega) v_{\mathbf{G}''}(\boldsymbol{q}) \chi_{\mathbf{G}'',\mathbf{G}'}(\boldsymbol{q}, \omega), \quad (2)$$

where v denotes the bare Coulomb potential kernel and $\chi^0_{\mathbf{G},\mathbf{G}'}(\boldsymbol{q}, \omega)$ is the noninteracting density response function, which is calculated by

$$\chi^0_{\mathbf{G},\mathbf{G}'}(\boldsymbol{q}, \omega) = \frac{2}{S} \sum_{\boldsymbol{k}_\parallel}^{\text{BZ}} \sum_{n} \sum_{n'} \frac{1}{\varepsilon_{\boldsymbol{k}_\parallel, n} - \varepsilon_{\boldsymbol{k}_\parallel + \boldsymbol{q}, n'} + \omega + i\delta} \times \langle \varphi_{\boldsymbol{k}_\parallel, n} | e^{-i(\boldsymbol{q}+\boldsymbol{G})\cdot \boldsymbol{r}} | \varphi_{\boldsymbol{k}_\parallel + \boldsymbol{q}, n'} \rangle \times \langle \varphi_{\boldsymbol{k}_\parallel + \boldsymbol{q}, n'} | e^{i(\boldsymbol{q}+\boldsymbol{G}')\cdot \boldsymbol{r}} | \varphi_{\boldsymbol{k}_\parallel, n} \rangle, \quad (3)$$

where $\varepsilon_{\boldsymbol{k},n}$ and $\varphi_{\boldsymbol{k},n}$ are the eigenvalues and eigenstates of the DFT self-consistent electronic Hamiltonian, respectively. $\boldsymbol{k}_\parallel$ is the wave vector in the 2D BZ. S represents the surface area and the factor of 2 is due to the spin. δ is a broadening parameter (here 5 meV). Note that by neglecting the lateral local field effects on the Be(0001) surface [16–18,59], only the $\boldsymbol{G} = \boldsymbol{G}' = 0$ component of the density response function is effective in solving Eqs. (2) and (3).

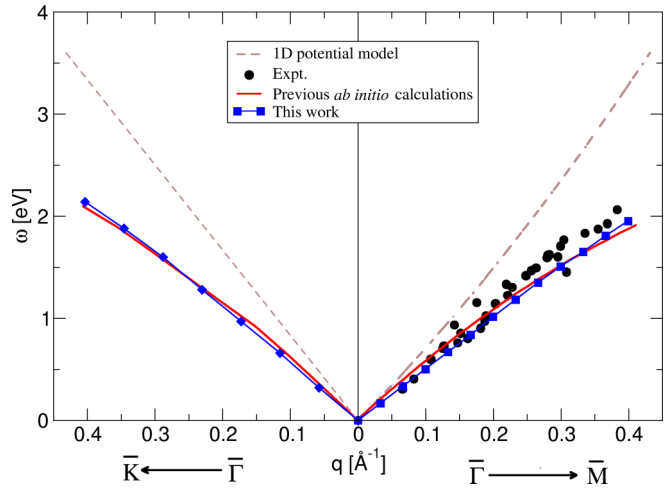

FIG. 1. The plasmon dispersion relationships along the $\bar{\Gamma}$-$\bar{M}$ and $\bar{\Gamma}$-$\bar{K}$ directions. The previous theoretical results derived by a 1D potential model [14,16–18] and the *ab initio* calculations [14,17] as well as the experimental results [14] are given for comparison.

Finally, the electron excitation rate $W(\omega, \boldsymbol{q})$ of the surface plasmons is obtained by taking the imaginary part of the surface response function $g(\omega, \boldsymbol{q})$, i.e.,

$$W(\omega, \boldsymbol{q}) = \text{Im}[g(\omega, \boldsymbol{q})]. \quad (4)$$

The plasmon dispersion relationship is then derived by determining the peak positions of $W(\omega, \boldsymbol{q})$.

Figure 1 shows the theoretically derived plasmon dispersion relationships as well as the experimental results. The calculated results almost exhibit a linear dispersion along the $\bar{\Gamma}$-$\bar{M}$ and $\bar{\Gamma}$-$\bar{K}$ directions with very low plasmon frequencies. Although the 1D potential model using a full nonlocal 3D dynamical screening is able to describe the strong localization of the electron and acoustic plasmons on the Be(0001) surface [17,18], it is evident that this isotropic model is insufficient to describe well the experimental plasmon dispersion relationships [14,16–18]. The obtained results from the 1D potential model represent the upper edge of the continuum for the electron-hole pair excitations within the surface states. By contrast, our *ab initio* derived plasmon dispersion relationships are in nice agreement with the experimental results [14] as well as previous *ab initio* calculations [14,17]. In particular, the anisotropy of the Be(0001) surface plasmon excitations along $\bar{\Gamma}$-$\bar{M}$ and $\bar{\Gamma}$-$\bar{K}$ are well captured by our *ab initio* calculations.

In order to uncover the underlying mechanism for the emergence of the acoustic surface plasmons on Be(0001), we calculated the surface band structure of Be(0001), as shown in Fig. 2(a). Our calculated surface band structure agrees well with the experimental data [22]. One can observe the twofold degenerated drumhead-like surface bands (i.e., DNSSs) close to the Fermi level, which essentially correspond to the topological boundary modes [60–64] induced by the band inversion between Be s-like and p_z-like orbitals [26].

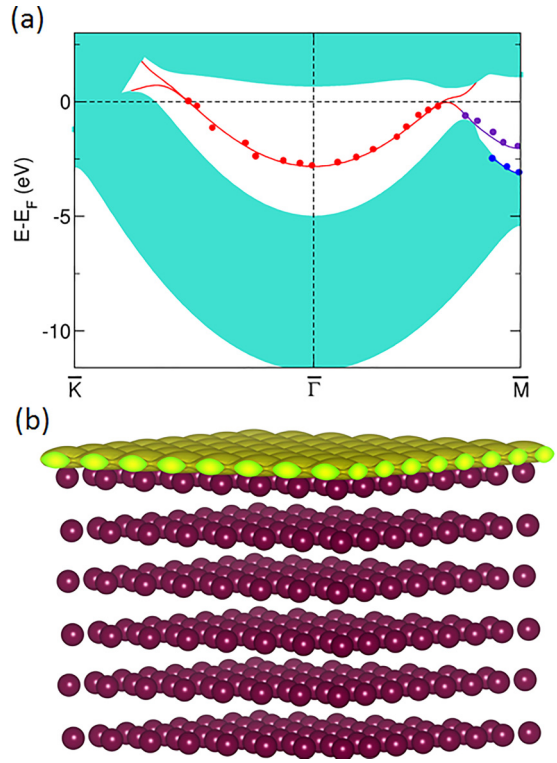

FIG. 2. (a) The surface band structures of Be(0001) and (b) the distribution of the DNSS charges on the Be(0001) surface. The points in (a) denote the experimental data obtained by the angular-resolved photoemission spectroscopy (ARPES) [22]. The green filled areas denote the bulk bands and the red curves indicate the DNSSs. The blue and purple curves near the $\bar{M}$ point arise from the surface oscillation of the topmost and second outer atomic layers, respectively.

These DNSSs are very distinct from the nearly free electrons on normal metal surfaces and can essentially be obtained from the Jackiw-Rebbi zero-energy solution of the boundary condition [65]. The DNSSs are partially occupied when the surface is electrically neutral and the particle-hole symmetry is considered. Also, these DNSSs are highly localized on the (0001) surface of Be, since they are composed of s- and p_z-like electronic states from the topmost atomic layer. As shown in Fig. 2(b), the DNSSs charges are localized at the single sheet clinging to the topmost atomic layer, in accordance with the low-energy acoustic plasmon excitations form of the Lindhard polynomials [14,16–18]. Furthermore, although the DNSSs appear to be parabolic, they are actually anisotropic along $\bar{\Gamma}$-$\bar{M}$ and $\bar{\Gamma}$-$\bar{K}$, as evidenced from Fig. 2(a). This may explain the anisotropy of the Be(0001) surface plasmon dispersion relationships. Therefore, one can expect that the DNSSs are likely to be the origin for the emergence of the low-energy acoustic surface plasmons on Be(0001), other than the commonly believed 2D-electron-gas-like Shockley surface states [17,18].

To prove this, we derived the momentum-dependent noninteracting density response functions and plasmon excitations rates. Four different momentum transfers $\boldsymbol{q}$ along $\bar{\Gamma}$-$\bar{M}$ were considered. The momentum-dependent noninteracting density response functions for each $\boldsymbol{q}$ at respective plasmon frequencies are shown in Figs. 3(a)–3(d). One can observe the typical arc states surrounding the $\bar{\Gamma}$ point, similar to the arc states for the electron-hole pair excitations within a surface parabolic band [19]. In addition, these arc states are much more bright than the other parts in the full surface Brillouin zone, indicating that the electron excitations at the **k** points on the arc states contribute the main parts to the surface noninteracting density response functions. From Fig. 2(a), it can be inferred that these arc states are intimately associated with the excitations of the DNSSs close to the Fermi level. Furthermore, it is obvious from Eqs. (1)–(3) that the plasmon excitations distribution and dispersion relationships are all determined by the surface noninteracting density response functions. Hence, calculating the contribution of the DNSSs to the surface noninteracting density response functions allows us to assess the effect of the DNSSs on the low-energy acoustic plasmons of the Be(0001) surface. To this end, we derived the plasmon excitations rates $W(\omega, \boldsymbol{q})$ of Be(0001) by disentangling the contribution of DNSSs to the acoustic surface plasmons from the states of the whole slab.

The results are compiled in Figs. 3(e)–3(h), and the experimental obtained angle-resolved electron energy loss spectra [14] are also shown in Figs. 3(i). One can see that under each momentum transfer, the derived plasmons excitations from the whole slab contain several peaks, whereas the plasmons excitations from DNSSs just show one dominant peak, which damps very fast to zero as the frequency increases. The plasmons excitations from DNSSs are in accordance with the plasmon excitations from parabolic-like bands. Then it can be inferred that the plasmon excitation peaks of the whole slab except the highest one have no relation with the DNSSs. Since their excitation energies are larger than that of the dominant peaks from DNSSs, these peaks can only belong to the excitations of the bands below DNSSs [see Fig. 2(a)], corresponding to the electrons in second outer or deeper atomic layers of the slab, which were not observed by the experimental surface measurement [see Fig. 3(i)]. Importantly, the highest peak positions of the plasmon excitation rates obtained from the whole slab, which determine the plasmon dispersion relationships, are almost identical with those from the DNSSs for all the considered momentum transfers. The highest main peak positions under each momentum transfer are located at 0.15, 0.31, 0.46, and 0.60 eV, respectively, thereby resulting in a low-energy linear dispersion relationship (Fig. 1). Besides, at the highest peaks for each momentum transfer, the DNSSs contribute the dominant parts to the plasmons excitations from the whole slab. This indicates that, for the plasmons from the whole slab, the main peaks are formed due to the excitations on DNSSs. As a result, it can be concluded that the anomalous low-energy and acoustic behaviors of the Be(0001) surface plasmons are indeed induced by the existence of DNSSs.

In summary, our study clearly demonstrates that the origin of the anomalous low-energy acoustic linear plasmon on the (0001) surface of Be is due to the topological bulk DNL induced DNSSs. Since the strongly localized and partially occupied DNSSs close to the Fermi level are very general for the topological DNL materials, the low-energy acoustic plasmons should be quite common for the topological semimetals with DNLs. Indeed, on the noble metal (111) surfaces, the low-energy acoustic surface plasmons have also been observed [66–68] and are most likely driven by the bulk DNLs

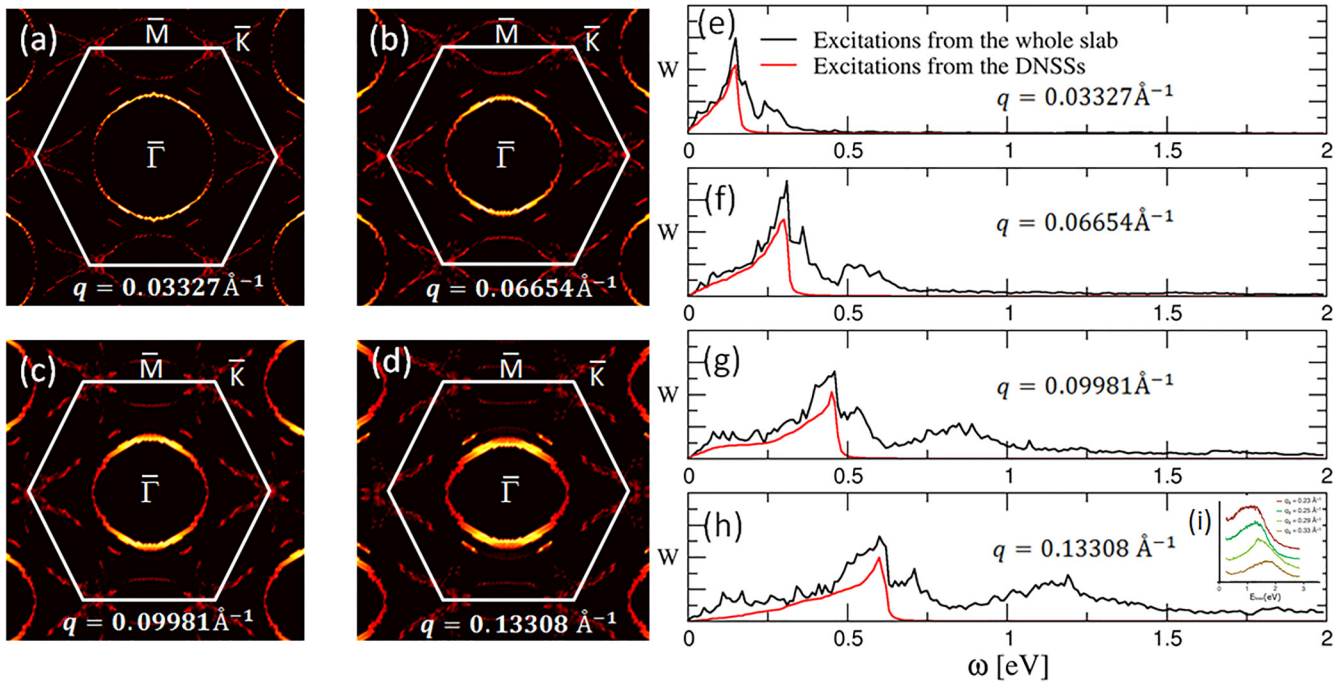

FIG. 3. (a)–(d) The imaginary part of the momentum-dependent noninteracting density response functions at the frequencies for plasmon excitation maximum of different $\boldsymbol{q}$ along the $\bar{\Gamma}$-$\bar{M}$ direction, and (e)–(h) the corresponding plasmon excitation rates. The bulk curves in (e)–(h) denote the plasmon excitations from the whole slab, while the red curves represent the plasmon excitations from the DNSSs only. The curves shown in (i) are the measured angle-resolved electron energy loss spectra [14].

as well, since their partially occupied Shockley surface states have been attributed to be the Rashba spin splitting DNSSs [69,70]. This work suggests a new route to obtain low-energy acoustic surface plasmons in the topological DNL semimetals.

This study was supported by the National Natural Science Foundation of China (Grants No. 52001308, No. 52188101, and No. 51725103), as well as the Key Project of the Chinese Academy of Sciences (Grant No. ZDRW-CN-2021-2-5).

[1] D. Pines and D. Bohm, Phys. Rev. **85**, 338 (1952).
[2] R. H. Ritchie, Phys. Rev. **106**, 874 (1957).
[3] H. Ishida, N. Shima, and M. Tsukada, Phys. Rev. B **32**, 6246 (1985).
[4] M. Rocca, Surf. Sci. Rep. **22**, 1 (1995).
[5] S. C. Schuster, R. V. Swanson, L. A. Alex, R. B. Bourret, and M. I. Simon, Nature (London) **365**, 343 (1993).
[6] G. Flatgen, K. Krischer, B. Pettinger, K. Doblhofer, H. Junkes, and G. Ertl, Science **269**, 668 (1995).
[7] W. L. Barnes, A. Dereux, T. W. L. A. A. Ebbesen, R. B. Bourret, and M. I. Simon, Nature (London) **424**, 824 (2003).
[8] H. J. Lezec, A. Degiron, E. Devaux, R. A. Linke, L. Martin-Moreno, F. J. Garcia-Vidal, and T. W. Ebbesen, Science **297**, 820 (2002).
[9] J. Pendry, Science **285**, 1687 (1999).
[10] F. Stern, Phys. Rev. Lett. **18**, 546 (1967).
[11] S. J. Allen, D. C. Tsui, and R. A. Logan, Phys. Rev. Lett. **38**, 980 (1977).
[12] T. Nagao, T. Hildebrandt, M. Henzler, and S. Hasegawa, Phys. Rev. Lett. **86**, 5747 (2001).
[13] N. March and M. Tosi, Adv. Phys. **44**, 299 (1995).
[14] B. Diaconescu, L. Vattuone, L. Savio, P. L. Hofmann, V. M. Silkin, J. M. Pitarke, E. V. Chulkov, E. V. Chulkov, P. M. Echenique, D. Farias, and M. Rocca, Nature (London) **448**, 57 (2007).
[15] S. Das Sarma and A. Madhukar, Phys. Rev. B **23**, 805 (1981).
[16] V. M. Silkin, A. Garcia-Lekue, J. M. Pitarke, E. V. Chulkov, E. Zaremba, and P. M. Echenique, Europhys. Lett. **66**, 260 (2004).
[17] J. M. Pitarke, V. U. Nazarov, V. M. Silkin, E. V. Chulkov, E. Zaremba, and P. M. Echenique, Phys. Rev. B **70**, 205403 (2004).
[18] V. M. Silkin, J. M. Pitarke, E. V. Chulkov, B. Diaconescu, K. Pohl, L. Vattuone, L. Savio, P. Hofmann, D. Farias, M. Rocca, and P. M. Echenique, Phys. Status Solidi A **205**, 1307 (2008).
[19] A. V. Chaplik, Sov. Phys. JETP **35**, 395 (1972).
[20] E. Plummer and J. Hannon, Prog. Surf. Sci. **46**, 149 (1994).
[21] U. Karlsson, S. Flodstr0m, R. Engelhardt, W. Gadeke, and E. Koch, Solid State Commun. **49**, 711 (1984).
[22] R. A. Bartynski, E. Jensen, T. Gustafsson, and E. W. Plummer, Phys. Rev. B **32**, 1921 (1985).
[23] L. I. Johansson, H. I. P. Johansson, J. N. Andersen, E. Lundgren, and R. Nyholm, Phys. Rev. Lett. **71**, 2453 (1993).
[24] P. J. Feibelman, Phys. Rev. B **46**, 2532 (1992).
[25] J. E. Inglesfield, Rep. Prog. Phys. **45**, 223 (1982).
[26] R. Li, H. Ma, X. Cheng, S. Wang, D. Li, Z. Zhang, Y. Li, and X.-Q. Chen, Phys. Rev. Lett. **117**, 096401 (2016).
[27] R. Li, J. Li, L. Wang, J. Liu, H. Ma, H.-F. Song, D. Li, Y. Li, and X.-Q. Chen, Phys. Rev. Lett. **123**, 136802 (2019).
[28] S. Das Sarma and E. H. Hwang, Phys. Rev. Lett. **102**, 206412 (2009).

[29] S. Raghu, S. B. Chung, X.-L. Qi, and S.-C. Zhang, Phys. Rev. Lett. **104**, 116401 (2010).
[30] S. Juergens, P. Michetti, and B. Trauzettel, Phys. Rev. Lett. **112**, 076804 (2014).
[31] D. E. Kharzeev, R. D. Pisarski, and H.-U. Yee, Phys. Rev. Lett. **115**, 236402 (2015).
[32] E. V. Gorbar, V. A. Miransky, I. A. Shovkovy, and P. O. Sukhachov, Phys. Rev. Lett. **118**, 127601 (2017).
[33] F. Zhang, J. Zhou, D. Xiao, and Y. Yao, Phys. Rev. Lett. **119**, 266804 (2017).
[34] J. Wang, X. Sui, S. Gao, W. Duan, F. Liu, and B. Huang, Phys. Rev. Lett. **123**, 206402 (2019).
[35] K. Sadhukhan, A. Politano, and A. Agarwal, Phys. Rev. Lett. **124**, 046803 (2020).
[36] A. Politano, V. M. Silkin, I. A. Nechaev, M. S. Vitiello, L. Viti, Z. S. Aliev, M. B. Babanly, G. Chiarello, P. M. Echenique, and E. V. Chulkov, Phys. Rev. Lett. **115**, 216802 (2015).
[37] A. Politano, G. Chiarello, B. Ghosh, K. Sadhukhan, C.-N. Kuo, C. S. Lue, V. Pellegrini, and A. Agarwal, Phys. Rev. Lett. **121**, 086804 (2018).
[38] A. Kogar, S. Vig, A. Thaler, M. H. Wong, Y. Xiao, D. Reig-i-Plessis, G. Y. Cho, T. Valla, Z. Pan, J. Schneeloch, R. Zhong, G. D. Gu, T. L. Hughes, G. J. MacDougall, T.-C. Chiang, and P. Abbamonte, Phys. Rev. Lett. **115**, 257402 (2015).
[39] A. Karch, Phys. Rev. B **83**, 245432 (2011).
[40] J. Zhou, H.-R. Chang, and D. Xiao, Phys. Rev. B **91**, 035114 (2015).
[41] J. Hofmann and S. Das Sarma, Phys. Rev. B **91**, 241108(R) (2015).
[42] J. C. W. Song and M. S. Rudner, Phys. Rev. B **96**, 205443 (2017).
[43] G. M. Andolina, F. M. D. Pellegrino, F. H. L. Koppens, and M. Polini, Phys. Rev. B **97**, 125431 (2018).
[44] C. Wang, Y. Sun, S. Huang, Q. Xing, G. Zhang, C. Song, F. Wang, Y. Xie, Y. Lei, Z. Sun, and H. Yan, Phys. Rev. Appl. **15**, 014010 (2021).
[45] M. Lv and S.-C. Zhang, Int. J. Mod. Phys. B **27**, 1350177 (2013).
[46] X. Jia, S. Zhang, R. Sankar, F.-C. Chou, W. Wang, K. Kempa, E. W. Plummer, J. Zhang, X. Zhu, and J. Guo, Phys. Rev. Lett. **119**, 136805 (2017).
[47] X. Jia, M. Wang, D. Yan, S. Xue, S. Zhang, J. Zhou, Y. Shi, X. Zhu, Y. Yao, and J. Guo, New J. Phys. **22**, 103032 (2020).
[48] P. Di Pietro, M. Ortolani, O. Limaj, A. Di Gaspare, V. Giliberti, F. Giorgianni, M. Brahlek, N. Bansal, N. Koirala, S. Oh, P. Calvani, and S. Lupi, Nat. Nanotechnol. **8**, 556 (2013).
[49] Y. D. Glinka, S. Babakiray, T. A. Johnson, M. B. Holcomb, and D. Lederman, Nat. Commun. **7**, 13054 (2016).
[50] X. Wen, V. Iyer, Y. P. Chen, and X. Xu, ACS Photonics **6**, 2492 (2019).
[51] S. Xue, M. Wang, Y. Li, S. Zhang, X. Jia, J. Zhou, Y. Shi, X. Zhu, Y. Yao, and J. Guo, Phys. Rev. Lett. **127**, 186802 (2021).
[52] P. Hohenberg and W. Kohn, Phys. Rev. **136**, B864 (1964).
[53] W. Kohn and L. J. Sham, Phys. Rev. **140**, A1133 (1965).
[54] G. Kresse and J. Furthmüller, Phys. Rev. B **54**, 11169 (1996).
[55] J. P. Perdew, K. Burke, and M. Ernzerhof, Phys. Rev. Lett. **77**, 3865 (1996).
[56] K. J. H. Mackay and N. A. Hill., J. Nucl. Mater. **8**, 263 (1963).
[57] M. Y. Chou, P. K. Lam, and M. L. Cohen, Phys. Rev. B **28**, 4179 (1983).
[58] B. N. J. Persson and E. Zaremba, Phys. Rev. B **31**, 1863 (1985).
[59] V. M. Silkin, E. V. Chulkov, and P. M. Echenique, Phys. Rev. Lett. **93**, 176801 (2004).
[60] M. Z. Hasan and C. L. Kane, Rev. Mod. Phys. **82**, 3045 (2010).
[61] X.-L. Qi and S.-C. Zhang, Rev. Mod. Phys. **83**, 1057 (2011).
[62] B. Yan and C. Felser, Annu. Rev. Condens. Matter Phys. **8**, 337 (2017).
[63] N. P. Armitage, E. J. Mele, and A. Vishwanath, Rev. Mod. Phys. **90**, 015001 (2018).
[64] H. Gao, J. W. Venderbos, Y. Kim, and A. M. Rappe, Annu. Rev. Mater. Res. **49**, 153 (2019).
[65] R. Jackiw and C. Rebbi, Phys. Rev. D **13**, 3398 (1976).
[66] M. Rocca, Li Yibing, F. Buatier de Mongeot, and U. Valbusa, Phys. Rev. B **52**, 14947 (1995).
[67] L. Vattuone, M. Smerieri, T. Langer, C. Tegenkamp, H. Pfnür, V. M. Silkin, E. V. Chulkov, P. M. Echenique, and M. Rocca, Phys. Rev. Lett. **110**, 127405 (2013).
[68] A. Politano, Plasmonics **8**, 357 (2013).
[69] B. Yan, B. Stadtmuller, N. Haag, S. Jakobs, J. Seidel, D. Jungkenn, S. Mathias, M. Cinchetti, M. Aeschlimann, and C. Felser, Nat. Commun. **6**, 10167 (2015).
[70] K. Yaji, A. Harasawa, K. Kuroda, R. Li, B. Yan, F. Komori, and S. Shin, Phys. Rev. B **98**, 041404(R) (2018).